Soils and Rocks
An International Journal of Geotechnical and Geoenvironmental Engineering
www.soilsandrocks.com
ISSN 1980-9743
ISSN-e 2675-5475

Numerical study on heat transfer performance of geothermal piles in a Brazilian sandy soil

Caique Roberto de Almeida[1], Cyro Albuquerque Neto[2], Cristina de Hollanda Cavalcanti Tsuha[3], Maria Eugenia Gimenez Boscov[1#]

Article

Keywords
Geothermal pile
Numerical model
TRT
Air conditioning
Energy consumption

Abstract

The worldwide consumption of electric energy destined for air conditioners, expected to triple by 2050, can be lessened by geothermal piles, which transfer heat from the internal environment of buildings to the subsoil. This paper shows the influence of pile geometry and properties of soil, pile, and pipe materials on the heat transfer of a geothermal pile to the surrounding soil, to support design from the viewpoint of thermal performance optimization. A numerical model was developed with ANSYS CFX 19.2, a high-performance Computational Fluid Dynamics tool, and calibrated using data from a thermal response test performed in a saturated sandy soil in São Paulo, Brazil. A parametric analysis was carried out varying pile length, diameter, and slenderness; soil and pile material conductivities; degree of saturation; fluid inlet temperature; fluid flow rate; and pipe thermal resistance. Results show that the fluid inlet temperature is the most influential parameter on the thermal performance of the pile. Heat transfer grows when geometrical parameters (diameter and length) are increased mainly due to an increase in heat exchange surface area, whereas the normalized heat transfer rate per unit of surface area of the pile is practically unaltered. Higher soil, pipe and pile thermal conductivities improve thermal performance. The degree of saturation increases the thermal conductivity of the soil; however, the effect is not remarkable on the system's thermal performance for saturation degrees higher than 20%. The fluid flow must be turbulent but increases above a certain flow rate do not improve the thermal performance.

1. Introduction

The worldwide use of air conditioners to refrigerate buildings consumed approximately 2,000 TWh of electric energy in 2018, a demand that tripled from 1990 to 2018. By 2050, this number is expected to exceed 6,000 TWh, with the most significant increases occurring in emerging economies with hottest climates (IEA, 2018). This increasing trend is enhanced by climate change (Hernandez Neto, 2020), since rising average temperatures will lead to a significant increase in CDDs (Cooling Degree Days) around the world, though at differing rates across regions: a 1 °C increase in global average temperature by 2050 may lead to an average increase in CDDs of 25% (IEA, 2018). The baseline scenario modeled by the International Energy Agency previews a rise in the number of individual cooling units or systems worldwide from just above 3.4 billion in 2016 to more than 8 billion in 2050 in the residential sector, and from 530 million to over 1.3 billion in the commercial sector (IEA, 2018).

Meanwhile, the worldwide use of geothermal energy increased from 8,664 MW to 70,329 MW between 1995 and 2015. Ground source heat pumps (GSHP) for air conditioning - piles, boreholes, closed or open loop systems - are responsible for 55.3% of the produced geothermal energy, a small contribution to the reduction of electrical energy consumption (IEA, 2018). Heating by geothermal piles started in Europe in 1984 (Brandl, 2006) and had an average increase of 10% per year in the following 20 years (Curtis et al., 2005).

In Brazil, the rise in average family income provided conditions for the ownership of household air conditioners to increase 9.0% per year from 2005 to 2017, consequently more than tripling electricity consumption for air conditioners (EPE, 2018). The electricity consumption for air conditioners

#Corresponding author. E-mail address: meboscov@usp.br
[1]Universidade de São Paulo, Department of Structural and Geotechnical Engineering, São Paulo, SP, Brasil.
[2]Centro Universitário FEI, Department of Mechanical Engineering, São Bernardo do Campo, SP, Brasil.
[3]Universidade de São Paulo, Department of Geotechnical Engineering, São Carlos, SP, Brasil.

Submitted on October 29, 2021; Final Acceptance on January 17, 2022; Discussion open until May 31, 2022.
https://doi.org/10.28927/SR.2022.076621

reached 18.7 TWh in 2017 and is predicted to reach 48.5 TWh in 2035.

Brazil is the ninth largest consumer of electrical energy in the world (Pereira et al., 2013). Geothermal energy in Brazil is mainly utilized for BRT (Bathing, Recreation and Tourism), PIS (Potential for Industrial use and Space heating) and TDB (Therapeutic, Drinking and Bathing). The contribution of geothermal energy to the overall Brazilian electrical energy generation, only 0.3% in 2012, is expected to reach 1% by 2040 (IEA, 2016).

In tropical climates, geothermal piles may take advantage of the deep foundations of buildings to dissipate thermal energy in superficial layers of soils (Loveridge & Powrie, 2013). However, research on the efficiency of energy piles to cool internal building temperatures in tropical climates is still limited. In Brazil, interest is still concentrated in the academy and the first case of geothermal piles for building conditioning was implanted in 2020 (Tsuha, 2020).

Some studies analyzed the potential of GSHP technology in Brazilian soils and climate. Morais et al. (2020) carried out a thermal response test (TRT) in a 12-m long geothermal pile of 0.25-m diameter installed in unsaturated lateritic clayey sand in São Carlos (SP), observing that performance was greatly affected by seasonality. Bandeira Neto (2015) tested 12-m long geothermal piles in the same soil, obtaining heat exchange rates by pile length of 79 W.m-1 to 110 W.m-1 for diameters ranging from 0.25 m and 0.50 m. These results were later employed by Orozco (2016) to formulate a numerical model in COMSOL Multiphysics software. Ferreira (2017) performed TRTs in a 12-m long geothermal pile of 0.4-m diameter installed in clayey soil in Campos dos Goytacazes (RJ) and concluded that, despite favorable soil thermal properties, the high undisturbed soil temperature made unfeasible the use of this technology to cool buildings interiors. Morais & Tsuha (2018) conducted a TRT in a 15-m long pile of 0.35-m diameter inserted in a sandy subsoil with high groundwater level (1.9 m below the surface) in São Paulo (SP) to obtain design parameters for the foundations of the CICS Living Lab building, which is the first case of use of geothermal piles in Brazil.

Ozudogru et al. (2014) developed and validated a numerical model of a TRT (0.45-m diameter and 20-m length) in sandy soil using COMSOL Multiphysics software. The adopted hypotheses were: conduction is the process that governs heat transfer in geothermal systems; heat transfer predominantly occurs in the radial direction; and the steel cage hardly influences heat exchange between pile and soil. Thompson III (2013) validated a numerical model based on a TRT performed in a 0.3-m diameter and 25-m geothermal pile in clayey and sandy soils, considering that the circulating fluid is incompressible and initial temperatures equal in the entire geothermal system.

This paper shows the results of numerical simulations carried out to investigate the heat transfer potential of geothermal piles as a function of pile geometry and involved materials, based on data from the TRT conducted by Morais & Tsuha (2018). The aim is to understand better the thermal performance of a geothermal pile considering local conditions of subsoil and climate.

2. Methods

The numerical model was developed in ANSYS CFX 19.2 Software, a Computational Fluid Dynamics (CFD) tool largely used in industry and in academic Multiphysics projects to solve complex problems with high-performance computing. The transport phenomena of heat transfer and fluid flow are represented by partial differential equations, and the CFX application uses the Finite Volume Method (FVM) as a form of discretization for the equations' solution (Maliska, 2004).

The numerical procedure followed two steps: (i) model validation, using experimental data from a TRT; and (ii) the parametric study, where the influence of the following parameters on pile performance were investigated: length, diameter and slenderness of the pile, pile and soil thermal conductivities, soil degree of saturation, fluid inlet temperature, fluid flow rate and pipe thermal resistance.

3. Experimental data: TRT

The TRT was performed by Morais & Tsuha (2018) on a 0.35-m diameter and 15-m long micropile (filled with grout) with a single U-loop (HDPE pipe with 32 mm external diameter and 26 mm internal diameter) during 10 days in February 2017 (Brazilian summer). 20-m deep prospection boreholes conveyed a soil profile composed of a thick layer of clayey sand covered by a 2.5-m layer of organic silt-sandy clay, and a borrow 1-m top layer of red to gray silt-sandy clay. The groundwater level depth, which varies from 2 to 4 m along the year, was 1.9 m during the test.

The undisturbed soil temperature was determined prior to the TRT by measuring the circulating water inlet and outlet temperatures without heat input into the system. During the test, a flow rate of 3.52×10-3 m3×s-1 and an applied power of 1,061 W or 70.8 W×m-1 (heat rate per unit length of pile) were used. Test results show that the heat rate injected into the pile was practically constant, variations in ambient temperature influenced the circulating fluid, and the geothermal system stabilized after 50 hours. Values obtained using the infinite line source theory were: λ (slope of the average temperature × log time curve = 1.99 with correlation coefficient $R2$ = 0.85, soil thermal conductivity K = 2.82 W×m-1×K-1, and soil thermal resistance rb = 0.13 m×K ×W-1. Table 1 shows the temperatures recorded during the TRT.

Table 1. Measured temperatures during the TRT (Morais & Tsuha, 2018).

TRT measurement	Value
Undisturbed ground temperature (K)	297.33
Average ambient temperature (K)	301.15
Maximum ambient temperature (K)	315.95
Minimum ambient temperature (K)	294.15
Tin 50 hours (K)	312.45
Tout 50 hours (K)	311.65
Tin 100 hours (K)	313.25
Tout 100 hours (K)	312.45
Tin 200 hours (K)	314.25
Tout 200 hours (K)	313.55
Flow rate (m×s-1)	0.66
Average heat power (kW)	1.06

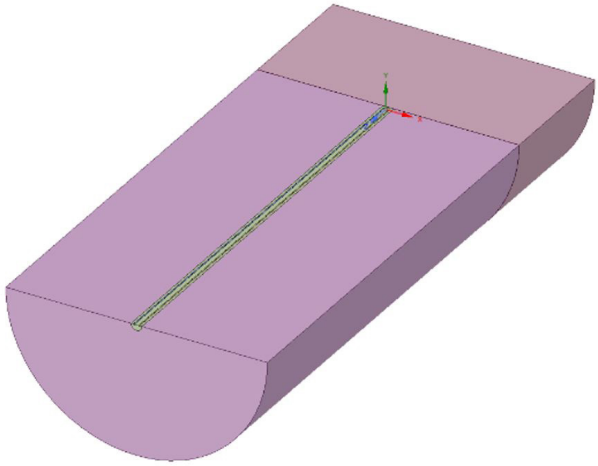

Figure 1. Geothermal pile geometry.

4. Numerical model

4.1 Geometry

The Space Claim module was used to create the geometry of the numerical model. The pile has a diameter of 0.35 m and a length of 15 m. The pipes have an inner diameter of 26 mm and an outer diameter of 32 mm. The bottom of the U loop was placed 10 cm above the pile tip. The steel cage was ignored since it has little influence on the heat exchange processes (You et al., 2017; Ozudogru et al., 2014). The soil was modeled as a continuous medium with cylindrical shape and 3-m radius (approximately 8.5 times the pile diameter), i.e., a distance large enough for the influence of pile heating on the soil to be negligible. Additionally, the model adopted a 3-m thick soil layer below the pile tip. The simulations were performed on a symmetrical half of the problem to decrease computational cost. Figure 1 illustrates the geothermal system geometry in ANSYS CFX.

4.2 Mesh

The mesh was created using the Meshing module. The mesh was refined inside the pipes, where there is circulating fluid, since the phenomena of turbulent water movement and forced convection make the modeling process more complex. The complexity of these phenomena also advises against the simplifying hypothesis of thermal energy flow in preferential directions, a fundamental condition for the choice of hexahedral elements. Therefore, tetrahedral elements, which are suitable for complex geometries such as the bottom of the U-loop, were used for the circulating fluid mesh. Tetrahedral elements also facilitate adjusting the mesh of transition zones compared to hexahedral elements. However, tetrahedral elements with different dimensions in pile and fluid must be matched to keep mesh connectivity

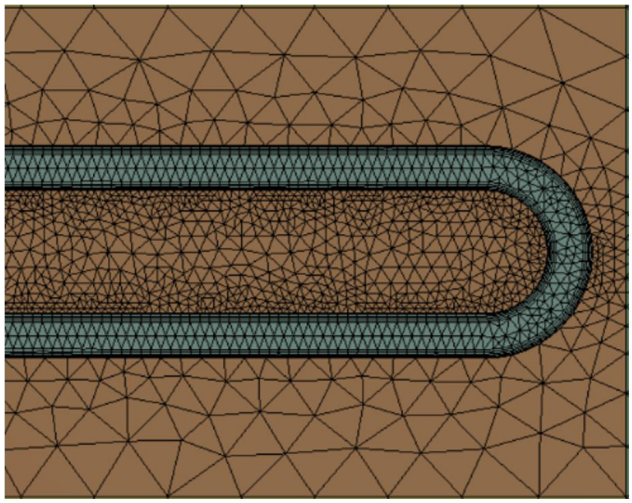

Figure 2. Transition mesh between fluid and grout.

and quality. The Inflation command generates prismatic elements to address connection problems and helps the user in the iterative process of restructuring previously defined tetrahedral elements to obtain adequate transitions. The space delimited by the surfaces of the HDPE pipes has 258,400 nodes and 551,765 elements. Figure 2 shows the mesh in the U-loop region.

Hexahedral elements (which form a mesh with fewer elements and reduce computational cost) were chosen to model the soil surrounding the pile. It is an acceptable choice since they are aligned in the direction of the thermal flow: radial heat transfer is the predominant mode of heat flow in a geothermal pile (Sani et al.,2019). As the surrounding soil mesh approaches the region where heat flow phenomena occur, smaller elements are necessary to guarantee a progressive refinement from the soil to the pile The surrounding soil geometry has

692,640 nodes and 661,248 elements. Figure 3 illustrates the ground mesh around the pile (XY axis).

Tetrahedral elements were used for the pile as the best configuration to meet the criterium of greater refinement (compared to the surrounding soil), also achieving an adequate transition between surrounding soil (coarser) and fluid mesh (more refined). The pile's central region, between the pipes, was more refined compared to the annular elements between soil and pipes because it is a transition between very refined regions (pipes). For the pile, 270,148 nodes and 1349,839 elements were used. Figure 4 illustrates the pile mesh in three-dimensional view.

For the soil geometry below the pile tip, the mesh should match the soil surrounding the pile and pile element (more refined), therefore, tetrahedral elements were used. Moreover, in this region energy flow does not occur predominantly in the radial direction, which rules out the use of hexahedral elements. The soil geometry below the pile has 50,042 nodes and 260,957 elements. Figure 5 shows the soil mesh at the bottom of the pile.

4.3 Turbulence model

The *k-ε* turbulence model was used in the Setup module. This model, commonly used in CFD simulations, is based on two equations representing the turbulent flow properties of turbulent kinetic energy (*kt*) and turbulent energy dissipation (εt), responsible for determining the turbulence scale.

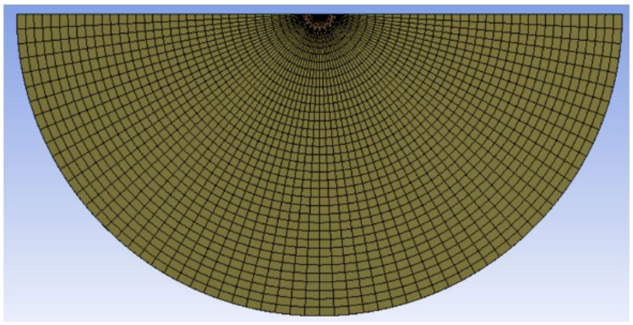

Figure 3. Detail of the soil mesh surrounding the geothermal pile.

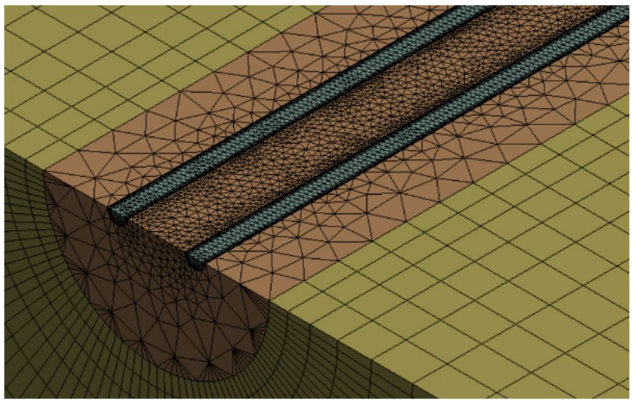

Figure 4. 3D meshes of the pile material, pipes, and soil.

4.4 Model validation

The TRT performed by Morais & Tsuha (2018) was used for the model validation. Three different times during the TRT were simulated; at each time, steady state condition was considered. The comparison was based on measured and simulated temperatures. A good fit in the validation phase indicates that the numerical model is reliable for parametric studies.

The parameters of the grout material were: density of 2400 kg×m-3, specific thermal capacity of 1000 J×kg-1×K-1, and thermal conductivity of 2.0 W×m-1×K-1. The HDPE pipes were simulated by a surface with a thermal resistance of 0.012 m2×K×W-1, calculated from a thickness of 6 mm and a thermal conductivity of 0.5 W×m-1×K-1 (ABNT, 2003; Orozco, 2016). Water properties at 25 °C are: density 997 kg×m-3, specific thermal capacity 4181.7 J×kg-1×K-1, and thermal conductivity 0.6069 W×m-1×K-1. The thermal conductivity of the soil estimated by the TRT was 2.82 W×m-1×K-1. The specific thermal capacity of the soil was estimated as 1578.9 J×kg-1×K-1 based on Lhendup et al. (2014).

The following boundary conditions were applied:

- Time t = 50 h: fluid inlet temperature 312.42 K, mass flow 0.3363 kg×s-1, ambient temperature 310.71 K, heating power 1031.20 W, undisturbed ground temperature 297.33 K (same for the three times);
- Time t = 100 h: fluid inlet temperature 313.26 K, mass flow 0.3366 kg×s-1, ambient temperature 311.16 K, heating power 1083.44 W;
- Time t = 200 h: fluid inlet temperature 314.29 K, mass flow rate 0.3663 kg×s-1, ambient temperature 313.10 K, heating power 1107.29 W.

Heat is exchanged by natural convection at the top of the geothermal system (adopted convection heat coefficient

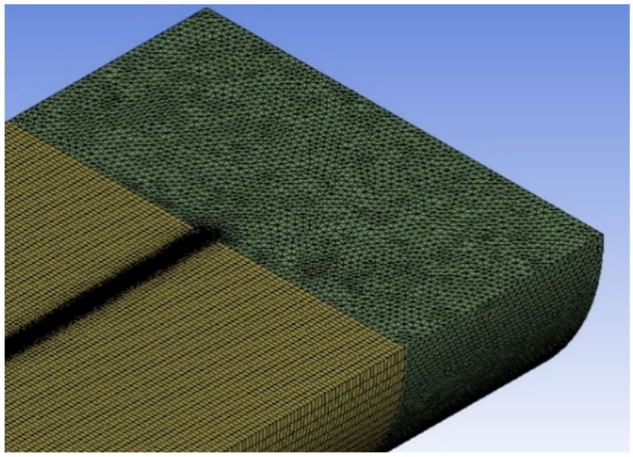

Figure 5. Mesh of the soil geometry below the pile tip.

of 10 W×m-2×K-1). In the outlet pipes the fluid is assumed to flow at atmospheric pressure. Soil temperature of 297.33 K (undisturbed ground temperature) was adopted for the distance of 3 m from the pile axis and at 3 m below the pile tip. Initially, the pile and soil temperatures are equal. Additionally, the soil limit domain is adiabatic; thus, all phenomena occur within the system composed of fluid, pipes, pile material and soil. Water circulates inside the pipes under turbulent flow conditions, Reynolds number equal to 17,109.

Table 2 compares experimental and numerical values of outlet temperature for the three times evaluated. The standard deviation for experimental temperatures was calculated considering the temperatures before and after (in a 1-minute interval) those measured at 50, 100 and 200 h. Combined uncertainty was calculated using Equation 1.

$$u_c^2 = u_i^2 + \sigma^2 \quad (1)$$

where: *uc* is the combined uncertainty, *ui* is the standard uncertainty (calculated as half of the PT-100 sensors' error limit) and σ is the standard deviation.

The deviations between numerical and experimental outlet temperatures are lower than the error limit of the PT-100 sensors (±0.5 K). The simulations based on the described parameters and conditions provided consistent numerical results when compared to the experimental results, therefore, the model was considered validated.

Figure 6 shows the values of total heat transfer rate obtained at the interfaces pipe/pile, pile/soil, soil/air and soil limit (radius of 3 m measured from the pile axis). The heat transfer rate at the pile/soil interface increased from 50 h (420.04 W) to 200 h (474.63 W), when the geothermal system stabilizes. This value of total heat transfer rate at the pile/soil interface under stable conditions indicates a relevant potential for thermal energy dissipation. Heat transfer rates at the pipe/pile interface are slightly higher than at the pile/soil interface. The soil limit presents a much higher rate (723.34 W at 200 h), due to the heat absorbed from the environment above the soil/pile system, where the air temperature is 313.1 K. This hypothesis is confirmed by the heat transfer rates at the soil/air interface, equivalent to the difference between the rates at the pipe/pile and soil limit interfaces. This phenomenon was observed in all stages of the parametric study.

Figure 7 shows the radial distribution of temperatures in a XY plane located at depth 7.5 m and time 200 h. Temperatures decrease as the radial distance from the pile center reaches the soil limit (undisturbed soil temperature = 297.3 K). Figure 8 illustrates the temperature distribution in a XZ plane (located at the pile center). The thermal influence zone's diameter (zone where the temperatures are at least 1 K higher than the undisturbed soil temperature) is 4.55m.

5. Parametric analysis

The basic scenario for the simulations consisted of the following parameters: 15 m length, 0.35 m diameter, grout thermal conductivity of 2 W×m-1×K-1, and soil thermal conductivity of 2.82 W×m-1×K-1.

5.1 Pile length

Pile lengths (*L*) of 5, 10, 15, 20, 30, and 50 m were simulated for a 0.35-m pile diameter. Increase in pile/soil heat exchange area increases the heat transfer rates at the pipe/pile, pile/soil, soil limit and soil/air interfaces (Figure 9a). However, Figure 10b shows that the heat transfer rate normalized by the pile surface area increases by 10% when the pile length increases from 5 to 50 m, but mostly until 20-m length. For piles longer than 20 m, increase in pile

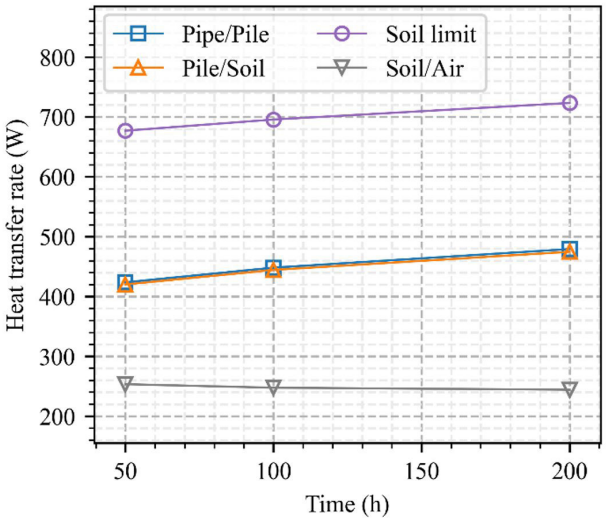

Figure 6. Heat transfer rate as a function of time at interfaces of the geothermal system.

Table 2. Combined uncertainty of numerical results.

Time	Experimental outlet temperature (K)	Numerical outlet temperature (K)	Deviation (K)	Combined uncertainty (±K)
50	311.7	311.6	0.1	0.3
100	312.5	312.7	-0.2	0.3
150	313.6	313.8	-0.2	0.3

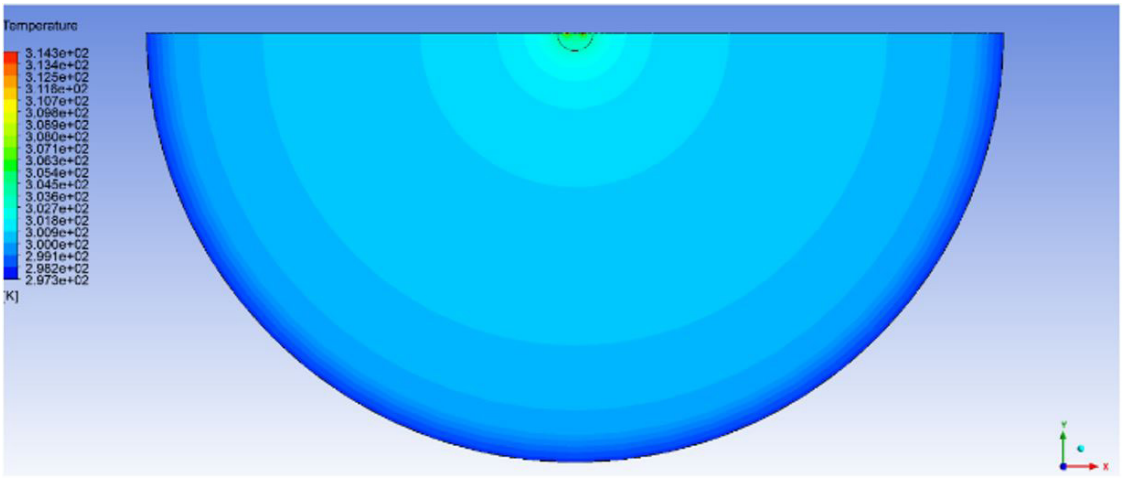

Figure 7. Radial distribution of temperatures in a XY plane at depth 7.5 m, time = 200 h.

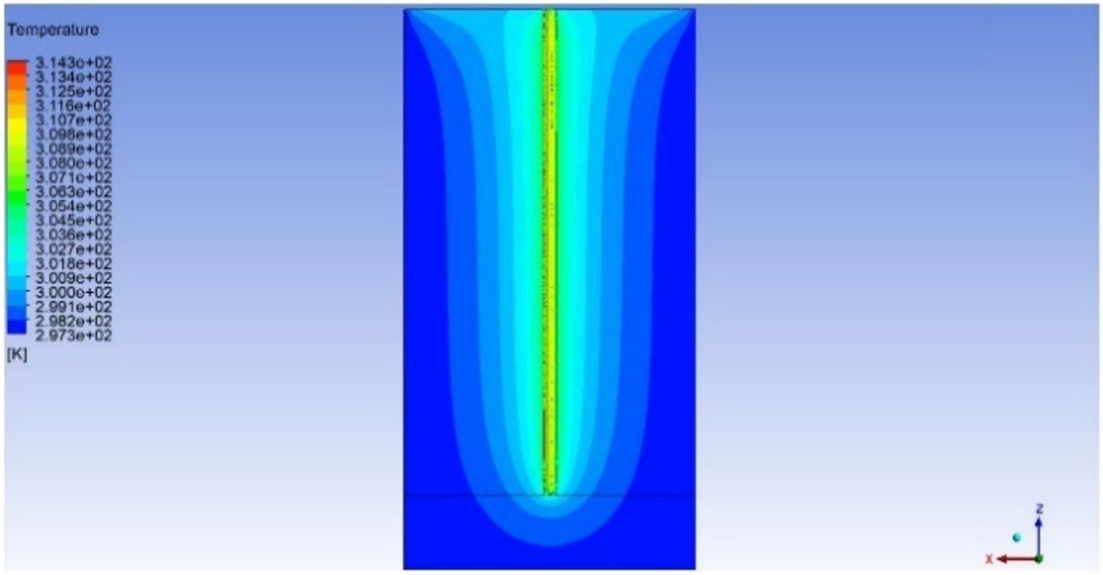

Figure 8. Distribution of temperatures in a XY plane located at the pile center, time = 200 h.

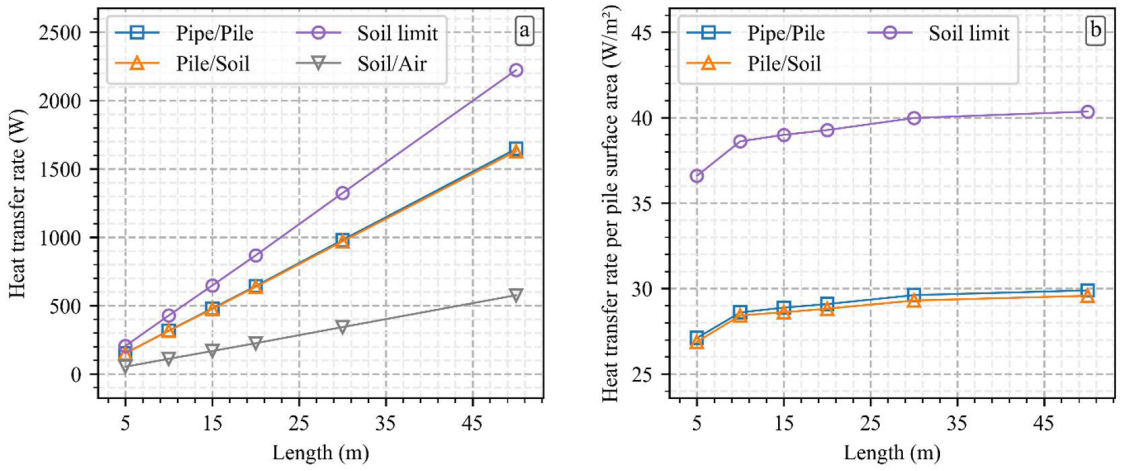

Figure 9. Heat transfer rate vs pile length: (a) total; (b) normalized by pile surface area.

length (consequently in pile surface) provides higher total heat exchanges (Figure 9a) but does not significantly improve the thermal efficiency per unit area.

5.2 Pile diameter

Pile diameters (D) of 0.2 m, 0.35 m, 0.50 m, 0.70 m, 0.90 m, and 1.1 m were simulated for a pile length of 15 m. The increase in diameter (and the consequent increase in the heat exchange area between pile and soil) allows an increase in heat transfer rate at the pipe/pile, pile/soil, soil/air and soil limit interfaces. Figure 10a shows the linear growth of the heat transfer rate with the increase of pile diameter. Figure 10b shows the variation of heat transfer rate normalized by pile surface area as a function of pile diameter. At the pile/soil interface, the normalized heat transfer rate increases by 7% when the diameter increases from 0.2 m to 1.1 m. For pile diameters larger than 0.35 m, the increase in diameter provides higher heat exchange, but the thermal efficiency of the pile per unit area of surface is little affected.

5.3 Pile slenderness

Pile slenderness index is given by L/D (Rotta Loria & Laloui, 2016). Two series were simulated: (1) varying pile length for a 0.35-m diameter pile, and (2) varying pile diameter of a 15-m long pile. The slenderness indexes for series (1) were: 14.3, 28.6, 42.9, 57.1, 85.7, and 142.9. Increase in the pile/soil heat exchange area causes an increase in total heat transfer rates at the interfaces: the heat transfer rate increases linearly with the pile slenderness index (Figure 11a). The slenderness indexes simulated for series (2) were: 11.8, 14.4, 18.6, 26.0, 37.1, and 65.0. In this case, L/D ratio increases with the decrease of pile diameter; consequently, the reduction of pile/soil heat exchange area causes a reduction of total heat transfer rates at the system

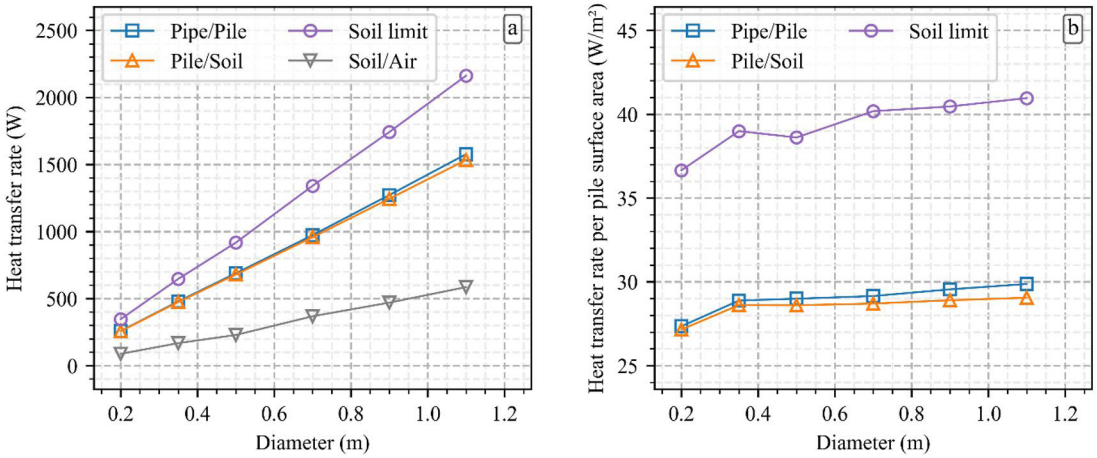

Figure 10. Heat transfer rate vs pile diameter: (a) total; (b) normalized by the pile surface area.

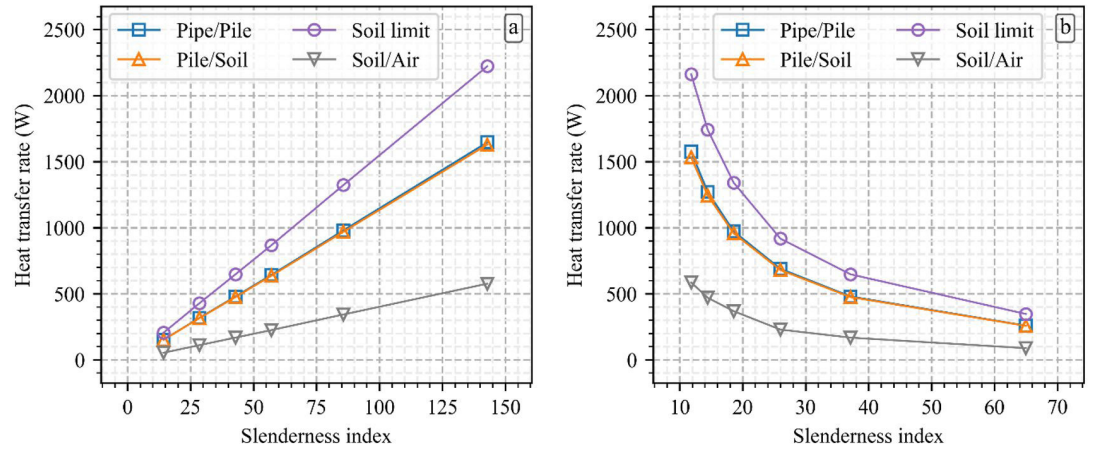

Figure 11. Heat transfer rate vs slenderness: (a) series 1; (b) series 2.

interfaces. Therefore, the heat transfer rate decreases with the increase of the slenderness index for a particular pile length (tending to asymptotes), as shown in Figure 11b. Comparison of Figures 11a and b indicates that the slenderness index is not an adequate indicator for the heat transfer rate of geothermal piles. The pile surface area controls the magnitude of total heat transfer rates. Thus, a particular slenderness index can be related to different values of pile surface area, which would result in different total heat transfer rates.

5.4 Thermal conductivity of the pile material

The grout conductivity varied from 0.17 W×m-1×K-1 (autoclaved cellular concrete) to 3.85 W×m-1.K-1 (GAM concrete; Asadi et al., 2018). For pipe/pile, pile/soil and soil limit interfaces, heat transfer rate increases with the increase in grout thermal conductivity, tending to asymptotes (Figure 12). Between the extreme grout thermal conductivity values, the heat transfer rate increased up to 3.6 times at the pile-soil interface. However, thermal conductivities higher than 4 W×m-1×K-1 apparently will not be accompanied by a further increase in heat transfer rates.

5.5 Soil thermal conductivity

Soil thermal conductivity varied from 0.9 to 3.7 W×m-1×K-1 - from clay to sandstone, respectively (Lhendup et al., 2014). Heat transfer rate at all interfaces increases with soil thermal conductivity (Figure 13). At the pile-soil interface, the heat transfer rate for sandstone is 2.3 times that for clay.

5.6 Saturation degree

Soil thermal conductivity values for different saturation degrees were based on Sánchez et al. (2015): 0.90 W×m-1×K-1 (s = 0.015), 1.35 W×m-1×K-1 (s = 0.188), 1.75 W×m-1×K-1 (s = 0.311), 2.10 W×m-1×K-1 (s = 0.480), 2.40 W×m-1×K-1 (s = 0.715), and 2.65 W×m-1×K-1 (s = 1.000). Heat transfer rates at the interfaces increased with soil saturation until a saturation degree of approximately 20%; further increases in saturation did not cause significant increase in heat transfer rates (Figure 14).

5.7 Fluid inlet temperature

Heat transfer rate increases linearly with the fluid inlet temperature at the pipe/pile, pile/soil and soil limit interfaces (Figure 15): as the fluid inlet temperature increases, the amount of heat injected into the geothermal system and the temperature gradient between the fluid and the rest of the

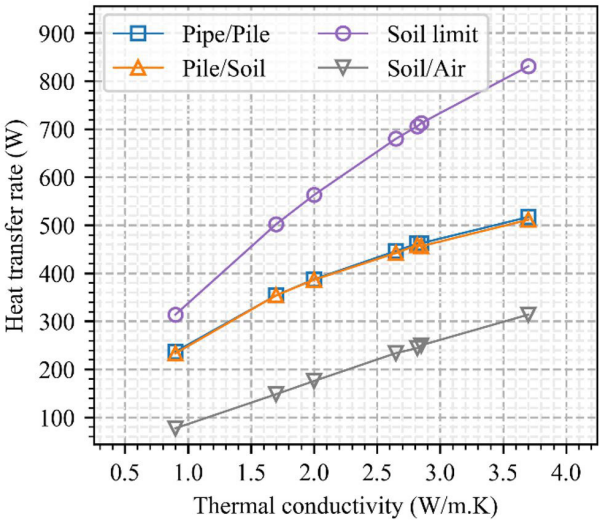

Figure 13. Heat transfer rate vs soil thermal conductivity.

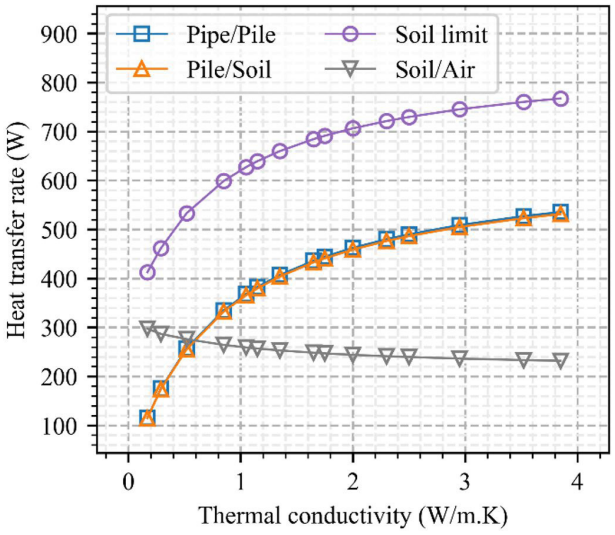

Figure 12. Heat transfer rate vs grout thermal conductivity.

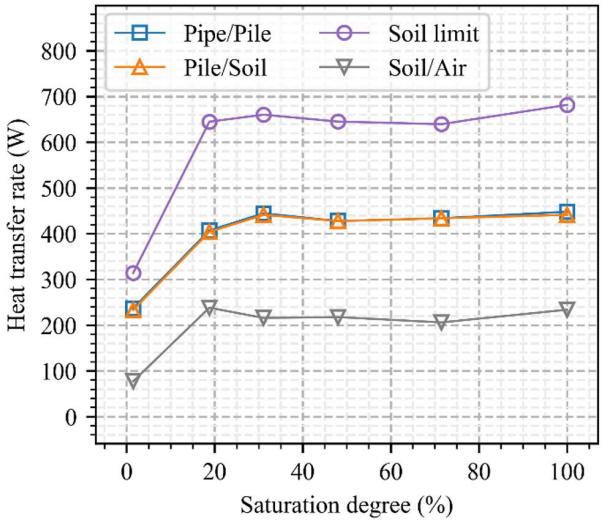

Figure 14. Heat transfer rate vs soil saturation degree.

system also increase. The difference between heat transfer rates at these interfaces decreases with increasing inlet temperature, and for inlet temperatures of approximately 360 K, such differences are lower than 50 K. The proximity among the curves in Figure 15 shows that the thermal exchanges with air in ambient temperature are not relevant as the fluid inlet temperature increases. This can be noticed at the soil/air interface: as the inlet temperatures increase the values of heat transfer rate decrease.

5.8 Fluid flow rate

Heat transfer rate exchanged between pile and soil sharply increases as flow rate increases until a value of approximately 10 L×min-1. However, further increases in flow rate do not result in higher heat transfer rates (Figure 16). The increase in heat transfer rate with fluid flow rate can be explained by the relation between the Nusselt number (Equation 2), which represents the gain in terms of heat transfer resulting from the convection/conduction ratio in a fluid, and the Reynolds number (Equation 3). Increasing the velocity of the circulating fluid increases the Reynolds number, which increases the Nusselt number. This process induces greater effectiveness in terms of heat exchange by convection and increases the total heat transfer rates. On the other hand, higher flow rate values decrease the time interval in which the thermal exchanges between the fluid and pipe occur to the point that, in turbulent conditions, the high speeds result in constant heat transfer rates (Figure 16).

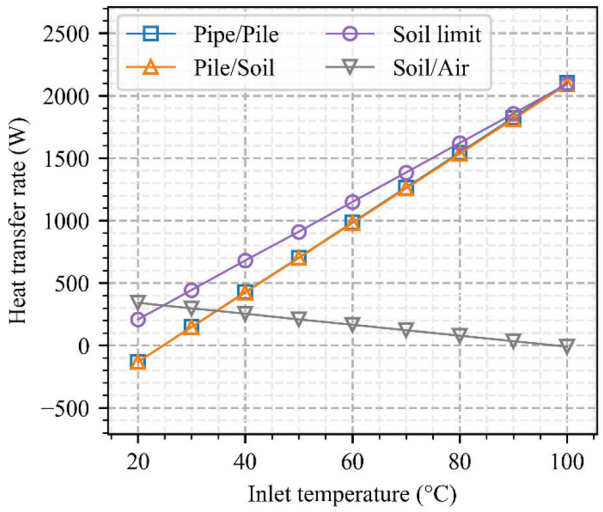

Figure 15. Heat transfer rate vs fluid inlet temperature.

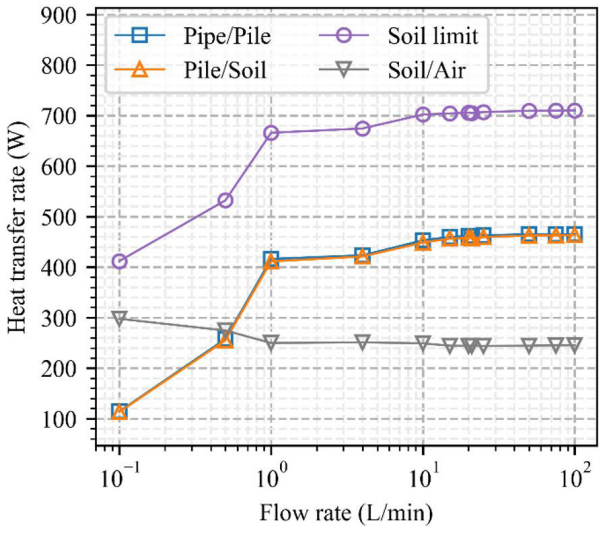

Figure 16. Heat transfer rate vs fluid flow rate.

$$Nu = \frac{hL_c}{k} \quad (2)$$

where: Nu = Nusselt number, h = coefficient of heat transfer by convection (W×m-2×K-1), Lc = characteristic length (m), and k = thermal conductivity (W×m-1×K-1).

$$Re = \frac{uL_c}{\nu} \quad (3)$$

where: Re = Reynolds number, u = flow speed (m.s-1), Lc = characteristic length (m), and ν = the kinematic viscosity of the fluid (m2×s).

5.9 Thermal resistance of pipe material

The influence of material and thickness of the pipes on the thermal efficiency of the geothermal pile was investigated by attributing different values of contact thermal resistance at the pipe-pile interface, as presented in Table 3. The increase in thermal contact resistance causes reduction of heat transfer rate values (the greater the thermal contact resistance, the greater is the difficulty imposed on the heat flow), as shown in Figure 17. Materials with higher thermal conductivities provided higher heat transfer rates, such as steel (R = 0.00012 m2×K ×W-1 and e = 6 mm, with a heat transfer rate 605.10 W at the grout/soil interface). On the other hand, materials with higher thermal contact resistances caused lower heat transfer rates, such as high density polyethylene (R = 0.048 m2×K ×W-1 and e = 24 mm, with a heat transfer rate of 265.51 W at the grout/soil interface). For null contact thermal resistances at the pipe/pile interface, a heat transfer rate of 607.01 W was obtained, which is the maximum heat transfer rate that the geothermal system could provide under these specified conditions of geometry and materials.

Table 3. Pipe materials and corresponding thermal resistivity.

w

Material	*K* (W.m-1.K-1)	*e* (mm)	*R* (m2.K.W-1)
PVC	0.17	6	0.0353
HDPE	0.50	3	0.0060
HDPE	0.50	6	0.0120
HDPE	0.50	24	0.0480
HDPE	0.50	12	0.0240
Copper	380	6	1.57895.10-5
Steel	50	6	0.00012
CPVC	0.139	6	0.04317
PEX	0.51	6	0.01176
LDPE	0.33	6	0.01818
Polypropylene	0.22	6	0.02727

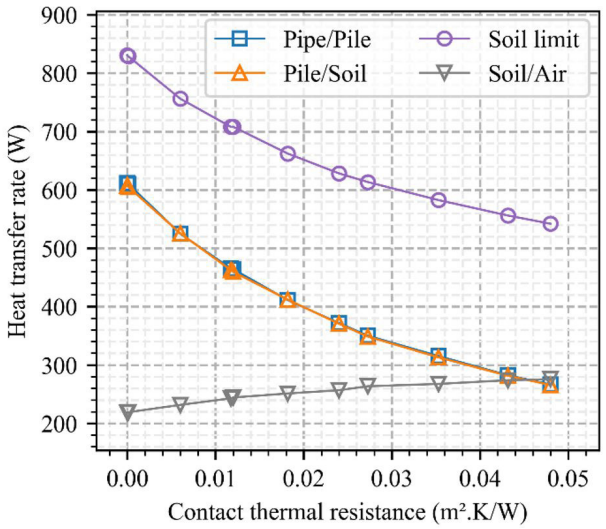

Figure 17. Heat transfer rate vs thermal resistance of the pipe.

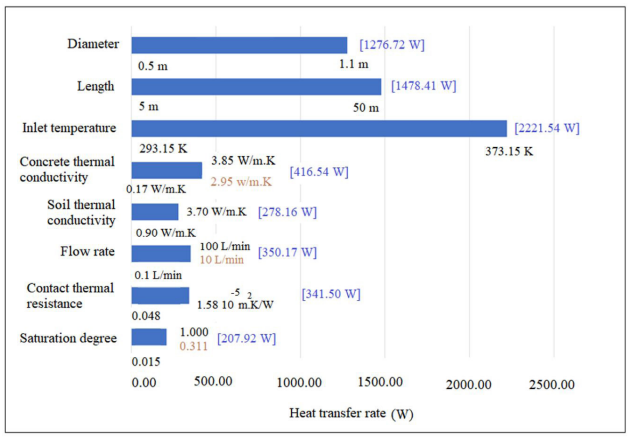

Figure 18. Heat transfer rate variations per analyzed parameters: maximum and minimum input values of each parameter in black, maximum heat transfer rates in blue, and input values for which heat transfer rates stabilize in brown.

5.10 Synthesis

Heat transfer rates at the pile/soil interface for the parameters evaluated in this study are presented in Figure 18. Fluid inlet temperature, pile diameter and pile length are the parameters that cause the highest increases in heat transfer rates. However, as previously discussed, pile length and diameter do not represent an actual increase in thermal efficiency, as normalized heat transfer rates per unit area are little impacted.

6. Final comments and conclusions

The experimental data from a TRT allowed the validation of a numerical model to analyze the thermal efficiency of a geothermal pile of 0.35-m diameter and 15-m length varying geometry and materials, based on heat transfer at the pipe/pile, pile/soil, soil limit and soil/air interfaces.

Results indicate that the normalized heat transfer rates per unit area do not increase varying pile length and diameter; however, as a consequence of higher heat exchange contact surface, total heat transfer rates increase with larger pile diameters or lengths.

Higher thermal conductivity of pile material results in better heat transfer performance. However, piles with thermal conductivities higher than 2.95 W×m-1×K-1 did not show a substantial increase in total heat transfer rates. For the pipes, the use of thermally conductive materials and reduction of thickness allow higher thermal exchanges between the circulating fluid and the rest of the geothermal system.

As the fluid inlet temperature increases, the temperature gradient between fluid and soil also increases, resulting in higher thermal efficiency. The fluid must circulate in turbulent regime, however for flow rates higher than 10 L×min-1 the values of total heat transfer rate stabilized.

Soil profiles with shallow groundwater levels are a desirable scenario for geothermal piles but heat transfer rates did not increase for saturation degrees higher than 20%. Soils with higher thermal conductivity provide higher total heat transfer rates in the geothermal system; however, subsoil thermal properties are not alterable. On the other hand, pile geometry, pile and pipe materials, and flow rate can be modified to provide an optimized design. Results indicate that there are optimal values of these parameters for the geothermal pile efficiency.

The numerical model also showed that the soil limit interface presents considerably higher heat transfer rates (because of the heat transfer rates provided by the above air temperature), while heat transfer rates at the pipe/pile and pile/soil interfaces are practically coincident, i.e., heat loss in the structural material is negligible.

Finally, numerical modelling of geothermal piles using ANSYS CFX contributed to a better understanding of the heat exchange performance of geothermal piles. Furthermore, numerical models are a powerful, low-cost, and useful tool

to properly design geothermal piles based on relatively few experimental data.

Acknowledgements

The authors are thankful to the Coordination to the Improvement of Higher Education Personnel (CAPES) for the master's scholarship grant number 88888.043643/2013-00.

Declaration of interest

The authors have no conflicts of interest to declare. All co-authors have observed and affirmed the contents of the paper and there is no financial interest to report.

Authors' contributions

Caique Roberto de Almeida: Investigation, Methodology, Formal Analysis, Validation, Writing – original draft. Cyro Albuquerque Neto: Methodology, Formal Analysis, Supervision. Cristina de Hollanda Cavalcanti Tsuha: Data curation. Maria Eugenia Gimenez Boscov: Conceptualization, Methodology, Formal Analysis, Supervision, Writing – review & editing.

List of symbols

h	Coefficient of heat transfer by convection
k	Thermal conductivity
kt	Turbulent kinetic energy
Lc	Characteristic length
u	Flow speed
εt	Turbulent energy dissipation
ν	Kinematic viscosity
CFD	Computational fluid dynamics
GSHP	Ground source heat pump
HDPE	High density polyethylene
MVF	Finite volumes method
Nu	Nusselt number
Re	Reynolds number
TRT	Thermal response test

References

Asadi, I., Shafigh, P., Hassan, Z.F.B.A., & Mahyuddin, N.B. (2018). Thermal conductivity of concrete: a review. *Journal of Building Engineering*, 20, 81-93. http://dx.doi.org/10.1016/j.jobe.2018.07.002.

Associação Brasileira de Normas Técnicas – ABNT. (2003). *ABNT NBR 15220: thermal performance in buildings: terminology, symbols and units*. Rio de Janeiro: ABNT (in Portuguese).

Bandeira Neto, L.A. (2015). *An experimental study of the termal response of heat exchanger piles in unsaturated tropical soil* [Master's dissertation, University of São Paulo]. University of São Paulo's repository (in Portuguese). https://doi.org/10.11606/D.18.2016.tde-08042016-092147.

Brandl, H. (2006). Energy foundations and other thermo-active ground structures. *Geotechnique*, 56(2), 81-122. http://dx.doi.org/10.1680/geot.2006.56.2.81.

Curtis, R., Lund, J., Rybach, L., & Hellstrom, G. (2005). Ground source heat pumps: geothermal energy for anyone, anywhere: current worldwide activity. *Proceedings of the World Geothermal Congress* (pp. 24-29), Antalaya, Turkey. International Geothermal Association.

Empresa de Pesquisa Energética – EPE. (2018). Brazilian energy balance 2018. Rio de Janeiro: EPE. Retrieved in October 29, 2021, from https://www.epe.gov.br/en/publications/publications/brazilian-energy-balance/brazilian-energy-balance-2018

Ferreira, M.S. (2017). *Resposta termomecânica de estaca geotérmica* [Master's dissertation, State University of Norte Fluminense]. State University of Norte Fluminense's repository (in Portuguese). https://uenf.br/posgraduacao/engenharia-civil/dissertacoes-de-mestrado-2017-marina-de-souza-ferreira/

Hernandez Neto, A. (2020). Desempenho energético de edificações em cenário de aquecimento global. In *CICS Talks*, São Paulo (in Portuguese). Retrieved in October 29, 2021, from https://www.youtube.com/watch?v=iuGSbz_JQDU

International Energy Agency – IEA (2016). K*ey world energy statistics 2016*. Paris: OECD/IEA. https://doi.org/10.1787/key_energ_stat-2016-en.

International Energy Agency – IEA (2018). *The future of cooling: opportunities for energy-efficient air conditioning.* Paris: OECD/IEA. Retrieved in October 29, 2021, from https://www.iea.org/reports/the-future-of-cooling

Lhendup, T., Aye, L., & Fuller, R.J. (2014). In situ measurement of borehole thermal properties in Melbourne. *Applied Thermal Engineering*, 73(1), 287-293. http://dx.doi.org/10.1016/j.applthermaleng.2014.07.058.

Loveridge, F.A., & Powrie, W. (2013). Pile heat exchangers: thermal behaviour and interactions. *Proceedings of the Institution of Civil Engineers - Geotechnical Engineering*, 166(2), 178-196. http://dx.doi.org/10.1680/geng.11.00042.

Maliska, C.R. (2004). *Transferência de calor e mecânica dos fluídos computacional* (2a ed.). Rio de Janeiro: LTC (in Portuguese).

Morais, T.S.O., & Tsuha, C.H.C. (2018). In-situ measurements of the soil thermal properties for energy foundation applications in São Paulo, Brazil. *Izvestiia po Himiia*, 50, 34-41.

Morais, T.S.O., Tsuha, C.H.C., Neto, L.A.B., & Singh, R.M. (2020). Effects of seasonal variations on the thermal response of energy piles in an unsaturated Brazilian tropical soil. *Energy and Building*, 216, 109971. http://dx.doi.org/10.1016/j.enbuild.2020.109971.

Orozco, H.C. (2016). *Validação do ensaio TRT para estudo paramétrico da troca de calor de uma estaca de energia em um solo tropical* [Master's dissertation, University of Brasília]. Universidade of Brasília's repository (in Portuguese). Retrieved in October 29, 2021, from https://repositorio.unb.br/handle/10482/21124

Ozudogru, T.Y., Olgun, C.G., & Senol, A. (2014). 3D numerical modelling of vertical geothermal heat exchangers. *Geothermics*, 51, 312-324. http://dx.doi.org/10.1016/j.geothermics.2014.02.005.

Pereira, C.D., Lamberts, R. & Ghisi, E. (2013). *Nota técnica referente aos níveis mínimos de eficiência energética de condicionadores de ar no Brasil.* Florianópolis: CB3E – Centro Brasileiro de Eficiência Energética em Edificações (in Portuguese).

Rotta Loria, A.F., & Laloui, L. (2016). The interaction factor method for energy pile groups. *Computers and Geotechnics*, 80, 121-137. http://dx.doi.org/10.1016/j.compgeo.2016.07.002.

Sánchez, M., Akrouch, G.A., & Briaud, J.L. (2015). An experimental, analytical and numerical study on the thermal efficiency of energy piles in unsaturated soils. *Computers and Geotechnics*, 71, 207-220. http://dx.doi.org/10.1016/j.compgeo.2015.08.009.

Sani, A.K., Singh, R.M., Cavarretta, I., Tsuha, C.H.C., & Bhattacharya, S. (2019). Inlet and outlet pipe heat interaction in a contiguous flight auger (CFA) pile. In: A. Ferrari & L. Laloui (Eds.), *Energy geotechnics SEG 2018* (Springer Series in Geomechanics and Geoengineering). Cham: Springer. http://dx.doi.org/10.1007/978-3-319-99670-7_15.

Thompson III, W.H. (2013). *Numerical analysis of thermal behaviour and fluid flow in geothermal energy piles* [Master's dissertation, Virginia Polytechnic Institute and State University]. Virginia Tech's repository. Retrieved in October 29, 2021, from http://hdl.handle.net/10919/24013

Tsuha, C.H.C. (2020). Utilização de energia geotérmica superficial na climatização do Edifício CICS Living Lab. In *CICS Talks*, São Paulo (in Portuguese). Retrieved in October 29, 2021, from https://www.youtube.com/watch?v=Hr4LNMKP3mg

You, S., Cheng, X., Yu, C., & Dang, Z. (2017). Effects of groundwater flow on the transfer performance of energy piles: experimental and numerical analysis. *Energy and Building*, 155, 249-259. http://dx.doi.org/10.1016/j.enbuild.2017.09.023.